IEEE Open Journal of the Communications Society

Received XX Month, XXXX; revised XX Month, XXXX; accepted XX Month, XXXX; Date of publication XX Month, XXXX; date of current version 11 January, 2024.

Digital Object Identifier 10.1109/OJCOMS.2024.011100

Layered Generalized Adaptively Biased Optical OFDM for IM/DD OWC Systems

Zuhang Geng[1,2,3] *(Student Member, IEEE)*, Xinke Tang[3], AND Yuhan Dong[1,2,3] *(Senior Member, IEEE)*

[1]Shenzhen International Graduate School, Tsinghua University, Shenzhen 518055, China
[2]Department of Electronic Engineering, Tsinghua University, Beijing 100084, China
[3]Peng Cheng Laboratory, Shenzhen 518055, China

CORRESPONDING AUTHOR: Yuhan Dong (e-mail: dongyuhan@sz.tsinghua.edu.cn).

This work was supported in part by the GuangDong Basic and Applied Basic Research Foundation under Grant 2022A1515010209 and Shenzhen Natural Science Foundation under Grant JCYJ20200109143016563.

ABSTRACT Due to the high spectral efficiency and robustness against inter-symbol interference (ISI), orthogonal frequency division multiplexing (OFDM) is attracting increasing attention in sixth-generation (6G) optical wireless communication (OWC) systems. In this paper, based on generalized adaptively biased optical OFDM (GABO-OFDM), we propose a novel power and spectrally efficient scheme of layered GABO-OFDM (LGABO-OFDM). The subcarriers in LGABO-OFDM are divided into several layers and conveyed simultaneously. Each layer employs GABO-OFDM which adds an adaptive bias to generate nonnegative signals. The added bias is orthogonal to the occupied subcarriers in each layer, therefore the transmitted information can be recovered iteratively at the receiver side. Theoretical derivation demonstrates that LGABO-OFDM is more spectrally efficient than traditional asymmetrically clipped optical OFDM (ACO-OFDM) and hybrid ACO-OFDM (HACO-OFDM). In order to optimize the power efficiency and reduce bit error rate (BER), we novelly propose an optical power allocation method and the principle of subcarrier allocation of LGABO-OFDM after analyzing the statistical properties of the adaptive bias. Numerical results further suggest that the proposed LGABO-OFDM has lower BER and peak-to-average power ratio (PAPR) than its conventional counterparts, which demonstrates its high power efficiency and capability of resisting the nonlinear distortion.

INDEX TERMS Optical wireless communication (OWC), orthogonal frequency division multiplexing (OFDM), optical power allocation, power efficiency

I. Introduction

OPTICAL wireless communication (OWC) is attracting increasing interests in both industry and academia on its wide unlicensed bandwidth, high data rates and low latency, which is capable to meet the requirements for sixth-generation (6G) mobile communication networks [1]. Orthogonal frequency division multiplexing (OFDM) highly succeeded in radio frequency (RF) communications is also considered in OWC systems with the advantages of high spectral efficiency and capacity for resisting inter symbol interference (ISI) [2], [3]. However, most OWC systems typically adopt intensity modulation with direct detection (IM/DD) and limit the transmitted signals to be real-valued and nonnegative [4], therefore cannot directly adopt the OFDM schemes in RF systems. To ensure the real-valued and nonnegative signals, several techniques have been proposed and adopted [5]–[7]. Typically, Hermitian symmetry is adopted to generate real-valued output of inverse fast Fourier transform (IFFT) and several optical OFDM schemes have been proposed to make the transmitted signals nonnegative.

As one popular optical OFDM scheme, direct-current (DC) biased optical OFDM (DCO-OFDM) directly adds a DC bias to the bipolar OFDM signal to make it unipolar [8]. However, the added DC bias results in poor power efficiency and relatively high bit error rate (BER) for DCO-OFDM OWC systems. Another popular solution is asymmetrically

clipped optical OFDM (ACO-OFDM), which only modulates odd subcarriers and clips the negative part of time-domain signals after IFFT [9]. Similarly, pulse-amplitude-modulated discrete multitone (PAM-DMT) is proposed in [10] to only utilize the imaginary part of subcarriers and finally obtain symmetry output of IFFT. As an extension, a hybrid ACO-OFDM (HACO-OFDM) scheme is introduced by combining both ACO-OFDM and PAM-DMT [11], [12]. Similar to ACO-OFDM, however, both PAM-DMT and HACO-OFDM suffer low spectral efficiency. These prior works sacrifice either power efficiency or spectral efficiency to enable nonnegative signaling, which restricts their usage in some applications with demands for high data rate and energy saving.

Based on these prior works, some new optical OFDM schemes have been proposed to improve the spectral efficiency of OWC systems (see [13]–[19] and references therein). Layered ACO-OFDM (LACO-OFDM) combines and transmits L layers of ACO-OFDM signals simultaneously and increases the spectral efficiency by using $N(1-1/2^L)$ subcarriers where N is the total number of subcarriers [13]–[16]. Adaptively biased optical OFDM (ABO-OFDM) reserves 1/4 of the subcarriers and adds an adaptive bias to generate nonnegative time-domain signals [17]. In ABO-OFDM OWC systems, the transmitted information is able to be demodulated directly at the receiver since fast Fourier transform (FFT) of the adaptive bias only falls on the reserved subcarriers. Furthermore, generalized ABO-OFDM (GABO-OFDM) extends to reserve $1/m$ of the subcarriers for any positive integer m which is a factor of the number of subcarriers and increases the design flexibility and the spectral efficiency of ABO-OFDM [18], [19]. Hybrid PAM-DMT (HPAM-DMT) employs 2 layers of PAM-DMT and adds symmetric biases [20]. Based on LACO-OFDM, absolute value LACO-OFDM (ALACO-OFDM) utilizes several occupied subcarriers to transmit the signs of the time-domain signals of the remaining subcarriers in LACO-OFDM [21]. Similar to HACO-OFDM, hybrid ABO-OFDM (HABO-OFDM) combines ABO-OFDM and PAM-DMT [22], while triple-layer hybrid optical OFDM (THO-OFDM) combines 2-layer LACO-OFDM and 1-layer PAM-DMT [23].

In the aforementioned optical OFDM schemes, DCO-OFDM exhibits lower energy efficiency due to the addition of a substantial DC bias. ACO-OFDM, PAM-DMT, ABO-OFDM, HACO-OFDM, THO-OFDM, and HABO-OFDM can only utilize approximately 50%, 50%, 75%, 75%, 87.5%, and 87.5% of the spectral resources respectively, and still have room to improve their spectral efficiencies. Additionally, layered optical OFDM, including LACO-OFDM and ALACO-OFDM, require multiple layers to reach high spectral efficiency, which increases computational complexity significantly. In summary, there is an urgent need for design methodology for layered optical OFDM schemes that allow flexible adjustment of spectral resources across layers to meet the performance requirements of various communication scenarios.

In this paper, we aim to propose a novel optical OFDM scheme for OWC systems to further improve the power efficiency with the spectral efficiency close to DCO-OFDM and relatively low complexity. The major contributions are summarized as follows. 1) We propose a novel efficient layered GABO-OFDM (LGABO-OFDM) scheme for OWC systems by combining different layers of GABO-OFDM signals at the transmitter side. It is proved that the distortion caused by the adaptive bias in higher layer is orthogonal to signals transmitted in lower layers. As a result, the signals from different layers could be recovered iteratively at the receiver side. Thanks to the flexibility of subcarrier allocation, LGABO-OFDM is not a single O-OFDM scheme, but a series of layered O-OFDM schemes. 2) We theoretically prove the superiority of LGABO-OFDM in spectral efficiency and show that the complexity of LGABO-OFDM is lower than LACO-OFDM with the same spectral efficiency by utilizing fewer layers. 3) We propose a new model for the added adaptive bias, the method of power allocation, and the principle of subcarrier allocation in LGABO-OFDM to further improve the power efficiency by obtaining the optimal BER performance. 4) Numerical results show that the proposed LGABO-OFDM outperforms its counterparts when taking both power and spectral efficiency into account. Furthermore, numerical results also suggest that LGABO-OFDM has relatively lower peak-to-average power ratio (PAPR) and performs better when resisting the nonlinear distortion.

The rest of this paper is organized as follows. Section II introduces the transceiver of the proposed LGABO-OFDM. The spectral efficiency and computational complexity of LGABO-OFDM are discussed in Section III. The statistical properties of the adaptive bias and optical power allocation strategy are analyzed in Section IV. In Section V, a novel principle of subcarrier allocation in LGABO-OFDM to optimize the BER performance is proposed. Section VI presents the numerical results of BER and PAPR performance. Finally, the conclusions are drawn in Section VII.

II. Proposed Layered GABO-OFDM for OWC Systems

Fig. 1 shows an illustration of free-space OWC system. Authors in [24] proposed a channel model considering the joint effect of atmospheric turbulence and both fluctuations of position and angle-of-arrival. The received signal can be presented as

$$y_n = Rhs_n + w_n, \quad n = 0, 1, ..., N-1, \tag{1}$$

where R denotes the photo-detector (PD) responsitivity, h denotes the channel attenuation coefficient, s_n is the transmitted time-domain signal, N is the length of s_n, and w_n denotes the sum of shot noise and thermal noise which are modelled as additive white Gaussian noise (AWGN) [25], [26].

This article has been accepted for publication in IEEE Open Journal of the Communications Society. This is the author's version which has not been fully edited and content may change prior to final publication. Citation information: DOI 10.1109/OJCOMS.2024.3400316

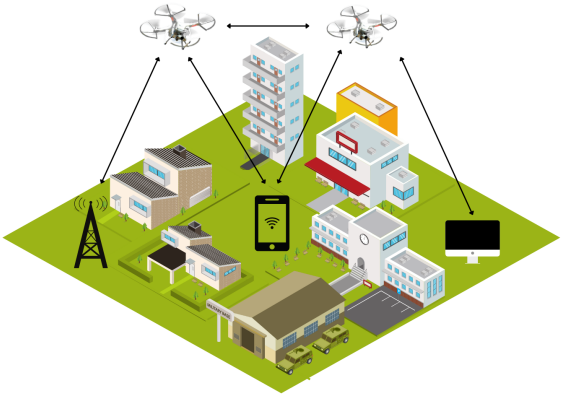

FIGURE 1. An illustration of free-space OWC system.

To improve the power efficiency, the proposed LGABO-OFDM divides the frequency-domain subcarriers into several layers. An adaptive bias is added in each layer to ensure nonnegative time-domain signals. Thanks to the character that the adaptive biases added in higher layers are orthogonal to signals in lower layers, the transmitted information can be recovered layer by layer with the proposed iterative receiver. Especially, when half of the available subcarriers are utilized in each layer, LGABO-OFDM reduces to be LACO-OFDM after normalizing optical power.

A. GABO-OFDM for IM/DD OWC Systems

In GABO-OFDM, adaptive biases are added in time domain to generate real-valued and nonnegative signals. To ensure the transmitted information fully recovered, the added biases are designed to be orthogonal to the occupied subcarriers in frequency domain. Fig. 2 depicts the transceiver of conventional GABO-OFDM scheme with N subcarriers for OWC systems. Since $1/m$ of the subcarriers are reserved while other subcarriers are utilized to convey symbols after modulation, the integer parameter m can determine the actual spectral efficiency. To eliminate the distortion caused by the adaptive bias, m is supposed to be a factor of N. The reserved subcarriers are chosen as $X_k = 0$ for $k = 0, m, 2m, \ldots, N-m$, where X_k denotes the frequency-domain GABO-OFDM signal at the k-th subcarrier. The time-domain signal x_n is generalized after Hermitian symmetry and IFFT as

$$x_n = \frac{1}{\sqrt{N}} \sum_{k=0}^{N-1} X_k \exp\left(j\frac{2\pi kn}{N}\right), \quad n = 0, 1, ..., N-1. \tag{2}$$

This time-domain signal is divided into N/m groups, i.e., $\left\{x_n, x_{n+\frac{N}{m}}, ..., x_{n+\frac{(m-1)N}{m}}\right\}, n = 0, 1, ..., N/m-1$, and each group contains m signal samples. To ensure x_n to be nonnegative and suitable for transmission, an adaptive bias is added. It has been proven that the distortion caused by

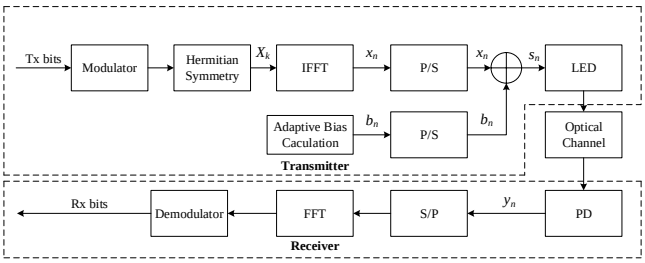

FIGURE 2. Block diagram of GABO-OFDM transceiver.

the adaptive bias is orthogonal to the transmitted information data symbols as long as the same bias is added to each signal sample in a group as

$$b_n = b_{n+\frac{N}{m}} = ... = b_{n+\frac{(m-1)N}{m}}, \quad n = 0, 1, ..., N/m-1, \tag{3}$$

where b_n denotes the adaptive bias added to the n-th signal sample in time domain. To guarantee power efficiency, the best adaptive bias is designed as

$$\begin{aligned} b_n &= b_{n+\frac{N}{m}} = ... = b_{n+\frac{(m-1)N}{m}} \\ &= -\min\left\{x_n, x_{n+\frac{N}{m}}, ..., x_{n+\frac{(m-1)N}{m}}\right\}. \end{aligned} \tag{4}$$

Then the transmitted time-domain signal s_n is expressed as

$$s_n = x_n + b_n, \quad n = 0, 1, ..., N-1. \tag{5}$$

At the receiver of a GABO-OFDM OWC system, a PD is employed to detect the optical signal and give the received signal y_n as

$$y_n = s_n + w_n, \quad n = 0, 1, ..., N-1. \tag{6}$$

The FFT output of b_n only falls on the reserved subcarriers, which has been proved in [18]. As a result, the transmitted information on other subcarriers could be recovered directly after FFT operation.

In conclusion, the key points of GABO-OFDM scheme can be summarized as follows. 1) Adaptive biases are added in time domain to generate real-valued and nonnegative signals. 2) It is proved that the added biases are orthogonal to the transmitted imformation, which ensures that the transmitted information is recoverable.

B. Transmitter of LGABO-OFDM Scheme

Different from LACO-OFDM, the number of subcarriers utilized to convey information in each layer of LGABO-OFDM scheme depends on the parameter m. Firstly, an array $\vec{m}$ is denoted as $\vec{m} = (m_1, m_2, ..., m_L)$, where m_l denotes the parameter m of GABO-OFDM in the l-th layer. The constraints of $\vec{m}$ are given by

$$\begin{cases} \mathrm{mod}(N, M_L) = 0, & (7) \\ \dfrac{N}{M_L} \geq 2, & (8) \end{cases}$$

where $\mathrm{mod}(\cdot,\cdot)$ denotes the modulo operator and $M_l = \prod_{i=1}^{l} m_i$. Especially, we define $M_0 = 1$. (7) ensures the

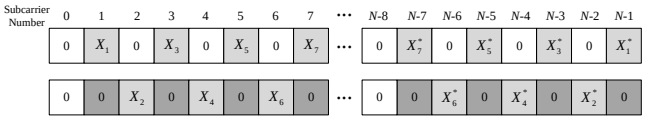

FIGURE 3. The subcarrier allocation of LGABO-OFDM with $\vec{m} = (2, 4)$.

orthogonality of the adaptive bias and transmitted symbols in each layer, while (8) results from the fact that X_0 and $X_{\frac{N}{2}}$ are supposed to be real-valued before IFFT operation at the transmitter side.

Fig. 3 takes LGABO-OFDM with $\vec{m} = (2, 4)$ as an example, illustrating subcarrier allocation at the transmitter side. The first layer utilizes half of the available subcarriers, specifically transmitting data symbols on the odd subcarriers. The second layer employs $\frac{3}{4}$ of the remaining available subcarriers and leaves $\frac{1}{4}$ unused. Therefore, $\frac{7}{8}$ of the subcarriers in frequency domain are divided into 2 layers and transmitted simultaneously.

Fig. 4 shows the block diagram of LGABO-OFDM signal generation part of the transmitter. By this, we emphasize the newly designed OFDM operation and simply omit the modulator, Hermitian symmetry, and P/S operations before OFDM. The 1st layer of LGABO-OFDM utilizes $\frac{m_1-1}{m_1}$ of N subcarriers and reserves the rest of subcarriers. Similarly, $\frac{m_2-1}{m_2}$ of the remaining subcarriers are used while the other $\frac{N}{m_1 m_2}$ subcarriers are reserved in the 2nd layer, and so on. In the l-th layer, $\frac{(m_l-1)N}{M_l}$ subcarriers are used while $\frac{N}{M_l}$ subcarriers are reserved. If the k-th subcarrier is utilized in the l-th layer, $k \in \mathbb{K}^{(l)}$, then $\mathrm{mod}(k, M_{l-1}) = 0$ and $\mathrm{mod}(k, M_l) \neq 0$. In addition, the utilized subcarriers in the l-th layer are expressed as

$$X_k^{(l)} = X_k, \quad k \in \mathbb{K}^{(l)}. \tag{9}$$

The IFFT output of the l-th layer is given by

$$\begin{aligned} x_n^{(l)} &= \frac{1}{\sqrt{N}} \sum_{k=0}^{\frac{N}{M_{l-1}}-1} X_{kM_{l-1}} \exp\left(j\frac{2\pi}{N} n M_{l-1} k\right) \\ &= \frac{\sqrt{M_{l-1}}}{M_{l-1}} \frac{1}{\sqrt{\frac{N}{M_{l-1}}}} \sum_{k'=0}^{\frac{N}{M_{l-1}}-1} X_{k'}^{(l)} \exp\left(j\frac{2\pi}{N/M_{l-1}} n k'\right) \\ &= \frac{\sqrt{M_{l-1}}}{M_{l-1}} x'^{(l)}_{\mathrm{mod}(n, N/M_{l-1})}, n = 0, 1, ..., N/M_{l-1} - 1, \end{aligned} \tag{10}$$

where $X_{k'}^{(l)}$ denotes the transmitted complex symbols in the l-th layer, and $x'^{(l)}_n$ denotes the $\frac{N}{M_{l-1}}$-point IFFT result of $X_{k'}^{(l)}$. It is obvious that $x_n^{(l)}$ is periodic, therefore the output of N-point IFFT in the l-th layer is able to be generated through a simple $\frac{N}{M_{l-1}}$-point IFFT operation, which reduces the computational complexity significantly.

To make time-domain signals nonnegative, the adaptive bias $b_n^{(l)}$ is adopted in the l-th layer. As mentioned above, the $\frac{N}{M_{l-1}}$-point IFFT result repeats M_{l-1} times in the l-th layer, then $b_n^{(l)}$ could be obtained with $x'^{(l)}_n$ rather than $x_n^{(l)}$ as

$$\begin{aligned} b_n'^{(l)} &= b'^{(l)}_{n+\frac{N}{M_l}} = ... = b'^{(l)}_{n+\frac{(m_l-1)N}{M_l}} \\ &= -\min\left\{x'^{(l)}_n, x'^{(l)}_{n+\frac{N}{M_l}}, ..., x'^{(l)}_{n+\frac{(m_l-1)N}{M_l}}\right\}, \\ & n = 0, 1, ..., N/M_l - 1, \end{aligned} \tag{11}$$

$$b_n^{(l)} = b'^{(l)}_{\mathrm{mod}(n, N/M_{l-1})}, \quad n = 0, 1, ..., N-1, \tag{12}$$

where calculating the minimum of m_l values is enough instead of M_l values.

As a result, the transmitted time-domain signal s_n is ultimately generated as

$$\begin{aligned} s_n &= x_n + b_n \\ &= \sum_{l=1}^{L} x_n^{(l)} + \sum_{l=1}^{L} b_n^{(l)}, \quad n = 0, 1, ..., N-1. \end{aligned} \tag{13}$$

C. Receiver of LGABO-OFDM Scheme

The received signal y_n in time domain and Y_k in frequency domain are respectively given by

$$\begin{aligned} y_n &= Rhs_n + w_n \\ &= Rh\left(\sum_{l=1}^{L} x_n^{(l)} + \sum_{l=1}^{L} b_n^{(l)}\right) + w_n, n = 0, 1, ..., N-1, \end{aligned} \tag{14}$$

$$Y_k = Rh\left(X_k + \sum_{l=1}^{L} B_k^{(l)}\right) + W_k, k = 0, 1, ..., N-1, \tag{15}$$

where Y_k, $B_k^{(l)}$, and W_k denote the N-point FFT results of y_n, $b_n^{(l)}$, and w_n, respectively. Then we obtain

$$\begin{aligned} Y_k' &= \frac{Y_k}{Rh} \\ &= X_k + \sum_{l=1}^{L} B_k^{(l)} + \frac{W_k}{Rh}, k = 0, 1, ..., N-1. \end{aligned} \tag{16}$$

It is clear that the key to recover the transmitted information is to figure out the impact of the adaptive bias b_n on the

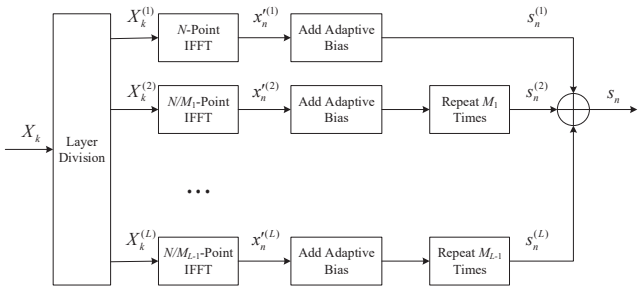

FIGURE 4. Block diagram of LGABO-OFDM signal generation part of the transmitter.

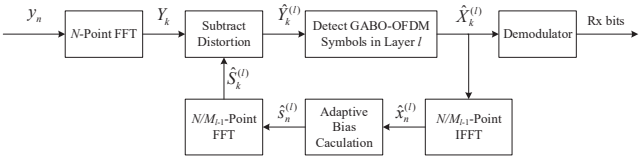

FIGURE 5. Block diagram of LGABO-OFDM signal processing part of the proposed iterative receiver.

frequency-domain signals. The FFT result of the adaptive bias in the l-th layer is given by

$$\begin{aligned} B_k^{(l)} &= \frac{1}{\sqrt{N}} \sum_{n=0}^{N-1} b_n^{(l)} \exp\left(-j\frac{2\pi kn}{N}\right) \\ &= \frac{1}{\sqrt{N}} \sum_{n=0}^{\frac{N}{M_l}-1} b_n^{(l)} \sum_{i=0}^{M_l-1} \exp\left(-j\frac{2\pi k}{N}\left(n+\frac{iN}{M_l}\right)\right) \\ &= \frac{1}{\sqrt{N}} \sum_{n=0}^{\frac{N}{M_l}-1} b_n^{(l)} \exp\left(-j\frac{2\pi kn}{N}\right) \sum_{i=0}^{M_l-1} \exp\left(-j\frac{2\pi ki}{M_l}\right), \\ & k = 0, 1, ..., N-1, \end{aligned} \tag{17}$$

where the second line of (17) is obtained by (11) and (12). When $\mathrm{mod}(k, M_l) = 0$, i.e., $k = 0, M_l, ..., N - M_l$, substituting k into (17), we can have

$$B_k^{(l)} = \frac{1}{\sqrt{N}} M_l \sum_{n=0}^{\frac{N}{M_l}-1} b_n^{(l)} \exp\left(-j\frac{2\pi kn}{N}\right). \tag{18}$$

If $\mathrm{mod}(k, M_l) \neq 0$, it has been proven in [18] that

$$B_k^{(l)} = 0. \tag{19}$$

Taking (18) and (19) into account, the distortion resulting from $b_n^{(l)}$ only falls on X_k for $k = 0, M_l, ..., N - M_l$, which are exactly the reserved subcarriers in the l-th layer. Therefore, the transmitted information can be recovered layer-by-layer by an iterative algorithm. Fig. 5 demonstrates the block diagram of LGABO-OFDM signal processing part of the proposed iterative receiver.

In the l-th layer, the distortion caused by the adaptive bias in higher layers is supposed to be removed from the received signal, which is expressed as

$$\hat{Y}_k^{(l)} = \begin{cases} Y_k', & l = 1 \\ Y_k' - \sum_{i=1}^{l-1} \hat{S}_k^{(i)}, & l \geq 2 \end{cases} \tag{20}$$

where $\hat{Y}_k^{(l)}$ denotes frequency-domain signal for demodulation in the l-th layer and $\hat{S}_k^{(i)}$ is the IFFT result of the estimated transmitted signal in the i-th layer.

Then the transmitted symbols in the l-th layer are directly detected as $\hat{X}_k^{(l)}$

$$\hat{X}_k^{(l)} = \arg \min_{X \in \Omega_{\mathrm{GABO}}} \left| X - \hat{Y}_k^{(l)} \right|, \tag{21}$$

where Ω_{GABO} denotes the constellation set of GABO-OFDM symbols and the $|\cdot|$ operator returns the absolute value. Then $\hat{X}_k^{(l)}$ can be adopted to estimate the time-domain signal $\hat{x}_n^{(l)}$, adaptive bias $\hat{b}_n^{(l)}$, and transmitted signal $\hat{s}_n^{(l)}$.

Considering the fact that only $\frac{(m_l-1)N}{M_l}$ subcarriers are occupied in the l-th layer, a simple N/M_{l-1}-point IFFT is sufficient to obtain $\hat{x}_n^{(l)}$. Then we could estimate $\hat{s}_n^{(l)}$ using the method mentioned in GABO-OFDM, generate $\hat{S}_k^{(l)}$ after an FFT operation, and estimate the distortion in the l-th layer. Repeating the operations above until the transmitted symbols in the final L-th layer are recovered, we can obtain all the desired information conveyed on $\left(1 - \frac{1}{M_L}\right) N$ subcarriers.

III. Spectral Efficiency and Computational Complexity

Complex tasks with high accuracy and data rate, such as high-definition (HD) real-time video transmission for disaster search and rescue, require high data rates and low complexity for OWC systems. In this section, we theoretically derive and analyze the spectral efficiency and computational complexity of the proposed LGABO-OFDM.

A. Spectral Efficiency

In LGABO-OFDM, there are $(N - N/M_L)$ subcarriers utilized to convey complex symbols generated by modulator. With the cyclic prefix simply omitted and quadrature amplitude modulation (QAM) adopted in LGABO-OFDM, the spectral efficiency is presented as

$$\begin{aligned} \eta_{\mathrm{LGABO-OFDM}} &= \frac{N - N/M_L}{2N} \log_2 N_Q \\ &= \frac{1 - 1/M_L}{2} \log_2 N_Q, \end{aligned} \tag{22}$$

where N_Q denotes the constellation number of QAM modulator.

In contrast, the spectral efficiency of some other optical OFDM schemes is shown as follows, where N_P-PAM and N_Q-QAM are adopted. DCO-OFDM utilizes $(N-1)$ subcarriers and has high spectral efficiency presented as

$$\begin{aligned} \eta_{\mathrm{DCO-OFDM}} &= \frac{N-1}{2N} \log_2 N_Q \\ &= \frac{1 - 1/N}{2} \log_2 N_Q. \end{aligned} \tag{23}$$

In ACO-OFDM, only half of the subcarriers are occupied while other subcarriers are reserved. Therefore, the spectral efficiency is given by

$$\eta_{\mathrm{ACO-OFDM}} = \frac{N/2}{2N} \log_2 N_Q = \frac{1}{4} \log_2 N_Q. \tag{24}$$

For HACO-OFDM, $N/2$ subcarriers convey complex-valued symbols while other $(N/2-2)$ subcarriers convey imaginary-valued symbols, which leads to the spectral efficiency presented as

$$\begin{aligned} \eta_{\mathrm{HACO-OFDM}} &= \frac{N/2}{2N} \log_2 N_Q + \frac{N/2-2}{2N} \log_2 N_P \\ &= \frac{1}{4} \log_2 N_Q + \frac{N/2-2}{2N} \log_2 N_P. \end{aligned} \tag{25}$$

LACO-OFDM and GABO-OFDM have relatively higher spectral efficiency by reserving $N/2^L$ and N/m subcarriers,

respectively, where L denotes the number of layers in LACO-OFDM and m denotes the number of divided groups in GABO-OFDM. Their spectral efficiencies are given by

$$\begin{aligned}\eta_{\mathrm{LACO-OFDM}} &= \frac{N - N/2^L}{2N}\log_2 N_Q \\ &= \frac{1 - 1/2^L}{2}\log_2 N_Q, \end{aligned} \tag{26}$$

$$\begin{aligned}\eta_{\mathrm{GABO-OFDM}} &= \frac{N - N/m}{2N}\log_2 N_Q \\ &= \frac{1 - 1/m}{2}\log_2 N_Q, \end{aligned} \tag{27}$$

It could be inferred that the proposed LGABO-OFDM is obviously superior to ACO-OFDM and HACO-OFDM in terms of spectral efficiency and can reach a spectral efficiency close to DCO-OFDM, which guarantees relatively high data rates for LGABO-OFDM OWC systems. Furthermore, to reach the same spectral efficiency as LACO-OFDM, LGABO-OFDM requires fewer layers on condition that $M_{L_1} = 2^{L_2}$, where L_1 and L_2 denote the number of layers of LGABO-OFDM and LACO-OFDM, respectively.

B. Computational Complexity

The primary sources of computational complexity of LGABO-OFDM scheme are attributed to the process of bias calculation and the implementation of IFFT and FFT operations.

In the context of bias calculation, we assume an LGABO-OFDM scheme with $\vec{m} = (m_1, m_2, ..., m_L)$ and $M_l = \prod_{i=1}^{l} m_i$ without loss of generality. In the l-th layer of this scheme, the time-domain signal is segmented into $\frac{N}{M_l}$ groups, with each group comprising m_l values. To compute the minimum of m_l values for each group, $(m_l - 1)$ comparison operations are sufficient. Consequently, the computational complexity of bias calculation is obtained by

$$\begin{aligned}C_{\mathrm{BC,LGABO}} &= \sum_{l=1}^{L} \frac{N}{M_l}(m_l - 1) \\ &= \sum_{l=1}^{L} \left(\frac{N}{M_{l-1}} - \frac{N}{M_l}\right) \\ &= N\left(1 - \frac{1}{M_L}\right), \end{aligned} \tag{28}$$

which suggests that LGABO-OFDM schemes, characterized by identical spectral efficiency and an equivalent total number of subcarriers, share the same computational complexity from bias calculation. In contrast, $\frac{N}{2^{l-1}}$ comparison operations are required for asymmetric clipping in the l-th layer of LACO-OFDM schemes. Then the computational complexity of asymmetric clipping for LACO-OFDM is given by

$$\begin{aligned}C_{\mathrm{AC,LACO}} &= \sum_{l=1}^{L} \frac{N}{2^{l-1}} \\ &= 2N\left(1 - \frac{1}{2^L}\right). \end{aligned} \tag{29}$$

TABLE 1. Computational Complexity Comparison of Different O-OFDM Schemes

O-OFDM Schemes		Transmitter	Receiver
LACO-OFDM	L=6	$1.96875\mathsf{O}(N\log_2 N)$	$4.875\mathsf{O}(N\log_2 N)$
LGABO-OFDM	$\vec{m} = (4,4,4)$	$1.3125\mathsf{O}(N\log_2 N)$	$3.5\mathsf{O}(N\log_2 N)$
	$\vec{m} = (8,8)$	$1.125\mathsf{O}(N\log_2 N)$	$3\mathsf{O}(N\log_2 N)$
	$\vec{m} = (2,4,8)$	$1.625\mathsf{O}(N\log_2 N)$	$4\mathsf{O}(N\log_2 N)$

It implies that LGABO-OFDM schemes have much fewer comparison operations than LACO-OFDM at the transmitter side.

Then it can be deduced that the primary differences in the computational complexity of LGABO-OFDM schemes are caused by IFFT and FFT operations. At the transmitter side, given that only one N-point IFFT is utilized in conventional ACO-OFDM and GABO-OFDM, the complexity of these optical OFDM schemes could be expressed as $\mathsf{O}(N\log_2 N)$. Nevertheless, both LACO-OFDM and LGABO-OFDM divide the occupied subcarriers into several layers each requiring one IFFT of different number of points.

For L-layer LGABO-OFDM, the size of IFFT and FFT blocks in the l-th layer is

$$N^{(l)} = \frac{N}{M_{l-1}}. \tag{30}$$

As a result, the computational complexity of LGABO-OFDM at the transmitter is given by

$$\begin{aligned}C_{\mathrm{TX}} &= \sum_{l=1}^{L} \mathsf{O}\left(N^{(l)}\log_2 N^{(l)}\right) \\ &\approx \sum_{l=1}^{L} \frac{1}{M_{l-1}}\mathsf{O}\left(N\log_2 N\right). \end{aligned} \tag{31}$$

Similar to LACO-OFDM, the receiver of LGABO-OFDM utilizes an iterative method, which leads to higher computational complexity than ACO-OFDM and GABO-OFDM. In each layer of LGABO-OFDM, an FFT operation and an IFFT operation are expected with sizes of blocks given in (30). As a result, the computational complexity of LGABO-OFDM at the receiver is

$$\begin{aligned}C_{\mathrm{RX}} &= \mathsf{O}\left(N\log_2 N\right) + 2\sum_{l=1}^{L-1} \mathsf{O}\left(N^{(l)}\log_2 N^{(l)}\right) \\ &\approx \left(1 + 2\sum_{l=1}^{L-1} \frac{1}{M_{l-1}}\right)\mathsf{O}\left(N\log_2 N\right), \quad L \geq 2. \end{aligned} \tag{32}$$

It is worth mentioning that no extra latency is imposed at the transmitter since the IFFT operations in different layers could be implemented simultaneously.

Table 1 shows the computational complexity of LACO-OFDM with 6 layers and several LGABO-OFDM schemes, which all have $(1 - 1/2^6)N$ occupied subcarriers and the same spectral efficiency. It can be seen that LGABO-OFDM has lower computational complexity than LACO-OFDM in

evidence. It is also shown that fewer layers are required for LGABO-OFDM to realize the same spectral efficiency as its conventional counterpart, which accounts for the lower complexity of LGABO-OFDM.

In the following Section IV and V, we will further improve power efficiency with fixed spectral efficiency by optimizing the allocation of optical power and subcarriers over the layers of LGABO-OFDM.

IV. Analysis of Adaptive Bias and Optical Power Allocation

In this section, we analyze the mean and variance of the adaptive bias in each layer and propose the principle of optical power allocation in order to optimize the BER performance and power efficiency for OWC systems.

A. Adaptive Bias

For a large value of N, the time-domain signals before adding adaptive bias in each layer of LGABO-OFDM could be modelled as Gaussian random variables (RVs) with zero mean and variance of $\sigma_l^2 = E\{(x_n'^{(l)})^2\}$ according to the central limit theorem. As mentioned in (11) and (12), the adaptive bias is set to be the additive inverse of the minimum of time-domain values in each group. Nevertheless, each pair of the variables are not independent, then the mean and variance of $b_n^{(l)}$ could not be obtained by simply calculating the minimum of several independent Gaussian RVs. For instance, the frequency-domain and time-domain signals with $m_l = 8$ are presented in Fig. 6 and Fig. 7, respectively.

It indicates that both frequency-domain signal and time-domain signal are divided into $\log_2 m_l$ rows. Furthermore, each row in time domain is the IFFT output of the corresponding row in frequency domain. For instance, the 1st row in Fig. 6 contains odd available subcarriers, which leads to antisymmetric characteristics of the corresponding time-domain signal as

$$x'^{(l,1)}_{n+N^{(l)}/2} = -x'^{(l,1)}_n, \quad n = 0, 1, \ldots, N^{(l)}/2 - 1, \tag{33}$$

where $x'^{(l,1)}_n$ denotes the time-domain signal of the 1st row of the l-th layer in LGABO-OFDM. In a similar fashion, the time-domain signals of the 2nd and 3rd rows have periodic and antisymmetric characteristics, as shown in Fig 7. We model $\{z_k\}$ as N/M_l independent identically distributed Gaussian RVs with zero means, where $k = 1, 2, ..., m_l - 1$. In the l-th layer, the time-domain signal $x_n'^{(l)}$ is divided into m_l sets each containing N/M_l values as shown in Fig 7. We denote these set of values as $\left\{x_n'^{(l)}\right\}$, $\left\{x'^{(l)}_{n+N/M_l}\right\}$, ..., $\left\{x'^{(l)}_{n+7N/M_l}\right\}$, where $n = 0, 1, \ldots, N/M_l - 1$. As a result, each set of time-domain signal values could be regarded as the linear combination of a set of independent Gaussian RVs, which is shown as

$$\begin{bmatrix} \hat{x}_n'^{(l)} \\ \hat{x}'^{(l)}_{n+\frac{N}{M_l}} \\ \hat{x}'^{(l)}_{n+\frac{2N}{M_l}} \\ \hat{x}'^{(l)}_{n+\frac{3N}{M_l}} \\ \hat{x}'^{(l)}_{n+\frac{4N}{M_l}} \\ \hat{x}'^{(l)}_{n+\frac{5N}{M_l}} \\ \hat{x}'^{(l)}_{n+\frac{6N}{M_l}} \\ \hat{x}'^{(l)}_{n+\frac{7N}{M_l}} \end{bmatrix} = \begin{bmatrix} 1 & 0 & 0 & 0 & 1 & 0 & 1 \\ 0 & 1 & 0 & 0 & 0 & 1 & -1 \\ 0 & 0 & 1 & 0 & -1 & 0 & 1 \\ 0 & 0 & 0 & 1 & 0 & -1 & -1 \\ -1 & 0 & 0 & 0 & 1 & 0 & 1 \\ 0 & -1 & 0 & 0 & 0 & 1 & -1 \\ 0 & 0 & -1 & 0 & -1 & 0 & 1 \\ 0 & 0 & 0 & -1 & 0 & -1 & -1 \end{bmatrix} \begin{bmatrix} z_1 \\ z_2 \\ z_3 \\ z_4 \\ z_5 \\ z_6 \\ z_7 \end{bmatrix} \tag{34}$$

where $\hat{x}_n'^{(l)}$ denotes the modelled variable of $x_n'^{(l)}$. For other values of m_l, $\hat{x}_n'^{(l)}$ could be modelled similarly.

Therefore, the modelled adaptive bias $\hat{b}_n'^{(l)}$ is available by calculating the minimum of $\left\{\hat{x}'^{(l)}_{n+\frac{iN}{M_l}}\right\}, i = 0, 1, ..., m_l - 1$. Monte Carlo simulation results of the statistical properties of the modelled $\hat{b}_n'^{(l)}$ and the actual $b_n'^{(l)}$ in the l-th layer of LGABO-OFDM are presented in Fig. 8, respectively, where the variances of $\left\{x'^{(l)}_{n+\frac{iN}{M_l}}\right\}$ and $\left\{\hat{x}'^{(l)}_{n+\frac{iN}{M_l}}\right\}$ are normalized respectively. The parameter m_l varies from 2 to 32 and the size of IFFT blocks is set to be $N^{(l)} = 1024$.

It is shown that the proposed model fits the actual adaptive bias well. However, with the value of m_l increases, more obvious disparities imply that the statistical properties of $b_n'^{(l)}$ become less assessable. The disparities result from that the minimum size of IFFT blocks is $\frac{2N^{(l)}}{m_l}$, which is not large enough to generate Gaussian RVs in time domain.

For ease of presentation, we define $a_{m,\text{norm}}$ and $\sigma^2_{m,\text{norm}}$ as the mean and variance of $\hat{b}_n'^{(l)}$ in Fig. 8 with $m_l = m$, respectively. Especially, when $m_l = 2$, $a_{2,\text{norm}}$ and $\sigma^2_{2,\text{norm}}$ could be regarded as the mean and variance of $|Z|$, respectively, where Z denotes a Gaussian RV with zero mean and normalized variance. Additionally, they could be calculated by

$$a_{2,\text{norm}} = \int_0^\infty \frac{2}{\sqrt{2\pi}} \exp\left(\frac{-\xi^2}{2}\right) d\xi = \sqrt{\frac{2}{\pi}}, \tag{35}$$

$$\sigma^2_{2,\text{norm}} = E\left\{|Z|^2\right\} - \left(E\left\{|Z|\right\}\right)^2 = 1 - \frac{2}{\pi}. \tag{36}$$

B. Optical Power Allocation

As mentioned above, the time-domain signal $x_n^{(l)}$ could be modelled as a Gaussian RV with zero mean and variance of σ_l^2 while the statistical properties of $b_n^{(l)}$ are discussed in the last subsection. As a result, the optical power in the l-th layer is given by

$$P_{o,l} = E\left\{s_n^{(l)}\right\} = E\left\{x_n^{(l)} + b_n^{(l)}\right\} \approx 0 + \beta_l \sigma_l = \beta_l \sigma_l, \tag{37}$$

where $\mathrm{E}\{\cdot\}$ denotes the expectation operator while $\beta_l = a_{m_l,\text{norm}}$.

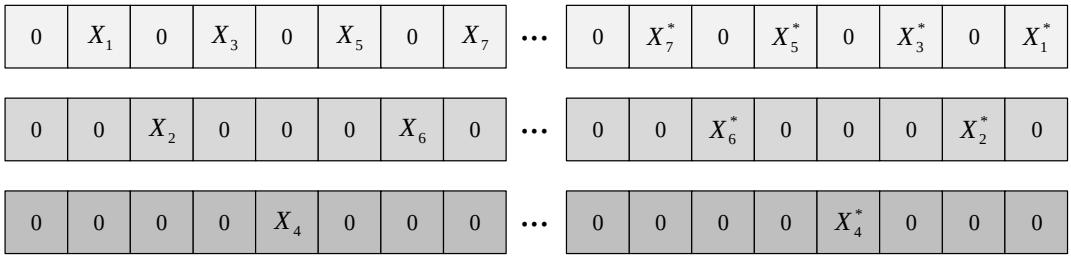

FIGURE 6. **The frequency-domain signal with $m_l = 8$ in LGABO-OFDM.**

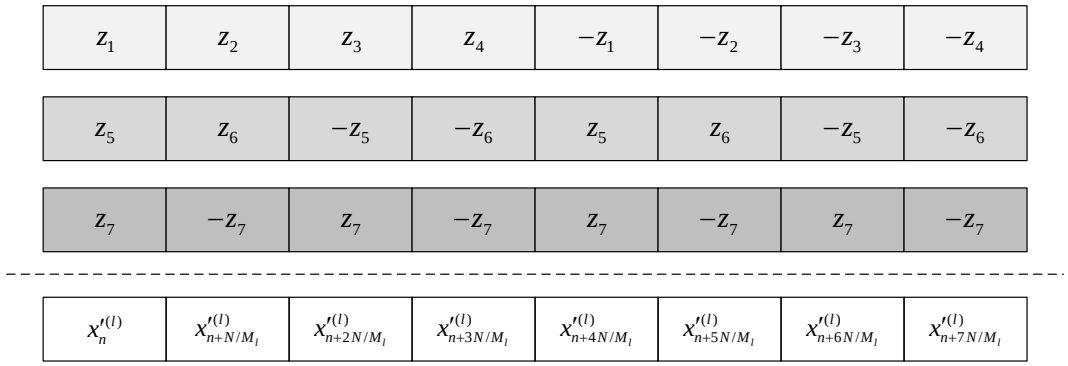

FIGURE 7. **The time-domain signal with $m_l = 8$ in LGABO-OFDM.**

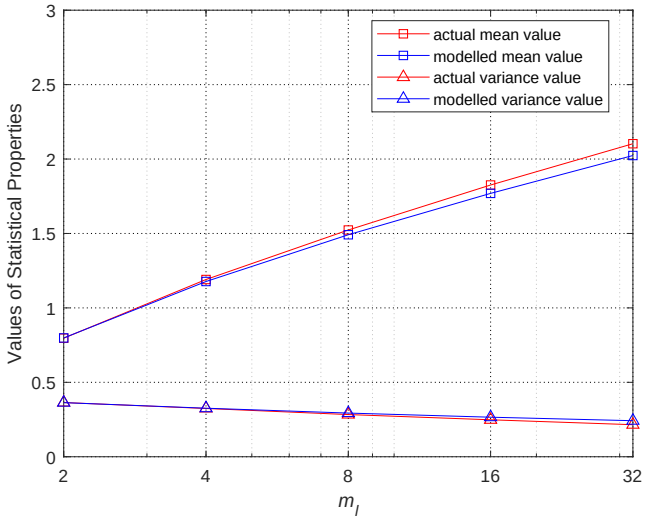

FIGURE 8. **Mean and variance of the modelled adaptive bias $\hat{b}_n'^{(l)}$ and the actual adaptive bias $b_n'^{(l)}$.**

Furthermore, by utilizing $\gamma_l = \sigma^2_{m_l,\mathrm{norm}}$, the electrical power of $s_n^{(l)}$ could be obtained by

$$\begin{aligned} P_{\mathrm{e},l} &= E\left\{\left|s_n^{(l)}\right|^2\right\} \\ &= E\left\{\left|x_n^{(l)}\right|^2 + 2x_n^{(l)}b_n^{(l)} + \left|b_n^{(l)}\right|^2\right\}. \end{aligned} \tag{38}$$

In Fig. 7, it indicates the antisymmetric characteristics of each row of time-domain signals $x_n'^{(l,i)}, i = 1, 2, \ldots, \log_2 m_l$. Therefore, the sum of values for bias calculation in each group $\left\{x_n'^{(l)}, x_{n+\frac{N}{M_l}}'^{(l)}, ..., x_{n+\frac{(m_l-1)N}{M_l}}'^{(l)}\right\}$ equals 0, which is presented as

$$\sum_{j=0}^{m_l-1} x_{n+j\frac{N}{M_l}}'^{(l)} = 0. \tag{39}$$

Then the adaptive bias is calculated as the opposite of the minimum of each group, as mentioned in (11). Using (39) and the periodicity of $x_n^{(l)}$ and $b_n^{(l)}$, we can obtain

$$\begin{aligned} E\left\{x_n^{(l)}b_n^{(l)}\right\} &= \frac{1}{N}\sum_{n=0}^{N-1} x_n^{(l)}b_n^{(l)} \\ &= \frac{M_{l-1}}{N}\sum_{n=0}^{\frac{N}{M_{l-1}}-1} x_n'^{(l)}b_n'^{(l)} \\ &= \frac{M_{l-1}}{N}\sum_{n=0}^{\frac{N}{M_l}-1}\sum_{j=0}^{m_l-1} x_{n+j\frac{N}{M_l}}'^{(l)}b_{n+j\frac{N}{M_l}}'^{(l)} \\ &= \frac{M_{l-1}}{N}\sum_{n=0}^{\frac{N}{M_l}-1} b_n'^{(l)}\sum_{j=0}^{m_l-1} x_{n+j\frac{N}{M_l}}'^{(l)} \\ &= 0, \end{aligned} \tag{40}$$

where the 4th equality results from the fact that the adaptive biases in the same group share the same value. After substituting (40) into (38), the electrical power of $s_n^{(l)}$ is calculated

by

$$\begin{aligned} P_{\mathrm{e},l} &= E\left\{\left|x_n^{(l)}\right|^2 + \left|b_n^{(l)}\right|^2\right\} \\ &= \sigma_l^2 + \left(\mathrm{var}\left\{b_n^{(l)}\right\} + \left|E\left\{b_n^{(l)}\right\}\right|^2\right) \\ &\approx \sigma_l^2 + \gamma_l\sigma_l^2 + \left(\beta_l\sigma_l\right)^2 \\ &= \left(1+\gamma_l+\beta_l^2\right)\sigma_l^2, \end{aligned} \tag{41}$$

where $\mathrm{var}\{X\}$ is the function calculating the variance of X.

It is worth mentioning that the desired transmitted signal is $x_n^{(l)}$, which is utilized to analyse the principle of optical power allocation rather than $s_n^{(l)}$ or $b_n^{(l)}$. In the l-th layer of LGABO-OFDM, the average electrical power of each occupied subcarrier in frequency domain is given by

$$E\left\{\left|X_k^{(l)}\right|^2\right\} = \frac{N\sigma_l^2}{N\left(m_l-1\right)/M_l} = \frac{M_l\sigma_l^2}{m_l-1}, \quad k \in \mathbb{K}^{(l)}. \tag{42}$$

In LGABO-OFDM OWC systems, the average optical power of the transmitted signals P_{o} is given by

$$P_{\mathrm{o}} = E\left\{s_n\right\} = \sum_{l=1}^{L} P_{\mathrm{o},l} = \sum_{l=1}^{L} \beta_l\sigma_l. \tag{43}$$

The shot noise and thermal noise falling on each subcarrier in frequency domain are modelled as AWGN with variance σ_w^2. Then the electrical SNR of the k-th subcarrier is denoted as SNR_k and presented in (44), with the assumption that the distortion caused by higher layers could be removed exactly before signals in lower layers are demodulated.

$$\mathrm{SNR}_k = \frac{E\left\{\left|X_k^{(l)}\right|^2\right\}}{\sigma_w^2} = \frac{M_l\sigma_l^2}{\left(m_l-1\right)\sigma_w^2}, \quad k \in \mathbb{K}^{(l)}. \tag{44}$$

In order to obtain the optimal BER performance, it is supposed to maximize the minimum SNR over all subcarriers which are occupied to transmit information with the constraint in (43). Therefore, the optimization problem could be presented as

$$\mathbf{P1}: \max_{\sigma_l} \quad \min_{k} \ \mathrm{SNR}_k \tag{45a}$$

$$\text{s.t.} \quad \mathrm{SNR}_k = \frac{M_l\sigma_l^2}{\left(m_l-1\right)\sigma_w^2}, \ k \in \mathbb{K}^{(l)}, \ 1 \le l \le L, \tag{45b}$$

$$\sum_{l=1}^{L} \beta_l\sigma_l = P_{\mathrm{o}}, \tag{45c}$$

$$\sigma_l \ge 0, \quad 1 \le l \le L. \tag{45d}$$

Let t denote the minimum of $\sqrt{\mathrm{SNR}_k}$, the optimization problem $\mathbf{P1}$ is transformed into

$$\mathbf{P2}: \min_{\sigma_l, t} \quad -t \tag{46a}$$

$$\text{s.t.} \quad \sqrt{\frac{M_l}{m_l-1}}\frac{\sigma_l}{\sigma_w} \ge t, \ k \in \mathbb{K}^{(l)}, \ 1 \le l \le L, \tag{46b}$$

$$\sum_{l=1}^{L} \beta_l\sigma_l = P_{\mathrm{o}}, \tag{46c}$$

$$t \ge 0. \tag{46d}$$

Especially, the optimization problem $\mathbf{P2}$ could be solved simply by utilizing Karush-Kuhn-Tucker (KKT) conditions. The Lagrange function and KKT conditions are given by

$$\begin{aligned} \mathcal{L} = &-t + \lambda\left(\sum_{l=1}^{L}\beta_l\sigma_l - P_{\mathrm{o}}\right) \\ &+ \sum_{l=1}^{L}\mu_l\left(t - \sqrt{\frac{M_l}{m_l-1}}\frac{\sigma_l}{\sigma_w}\right) - \mu t, \end{aligned} \tag{47}$$

$$\begin{cases} \dfrac{\partial\mathcal{L}}{\partial t} = -1 + \sum_{l=1}^{L}\mu_l - \mu = 0, & \text{(48a)} \\ \dfrac{\partial\mathcal{L}}{\partial\lambda} = \left(\sum_{l=1}^{L}\beta_l\sigma_l - P_{\mathrm{o}}\right) = 0, & \text{(48b)} \\ \dfrac{\partial\mathcal{L}}{\partial\sigma_l} = \lambda\beta_l - \sqrt{\dfrac{M_l}{m_l-1}}\dfrac{\mu_l}{\sigma_w} = 0, \ 1 \le l \le L, & \text{(48c)} \\ \mu_l\left(t - \sqrt{\dfrac{M_l}{m_l-1}}\dfrac{\sigma_l}{\sigma_w}\right) = 0, \ 1 \le l \le L, & \text{(48d)} \\ \mu t = 0, & \text{(48e)} \\ \mu_l \ge 0, \ 1 \le l \le L, & \text{(48f)} \\ \mu \ge 0. & \text{(48g)} \end{cases}$$

The solutions are presented as

$$\begin{cases} t = \dfrac{P_{\mathrm{o}}}{A\sigma_w}, & \text{(49a)} \\ \sigma_l = \sqrt{\dfrac{m_l-1}{M_l}}\dfrac{P_{\mathrm{o}}}{A}, & \text{(49b)} \\ \mu = 0, & \text{(49c)} \\ \mu_l = \sqrt{\dfrac{m_l-1}{M_l}}\dfrac{\beta_l}{A}, & \text{(49d)} \\ \lambda = \dfrac{1}{A\sigma_w}, & \text{(49e)} \end{cases}$$

where $A = \sum_{l=1}^{L}\frac{\beta_l}{\sqrt{M_l/(m_l-1)}}$. After substituting (49b) into (44), it could be inferred that

$$\mathrm{SNR}_k = \frac{P_{\mathrm{o}}^2}{A^2\sigma_w^2}, \tag{50}$$

which means that each occupied subcarrier in frequency has the same SNR performance of LGABO-OFDM.

The optical power in the l-th layer could be obtained by substituting (49b) into (37), which is shown as

$$P_{\mathrm{o},l} = \frac{\beta_l P_{\mathrm{o}}}{A\sqrt{M_l/\left(m_l-1\right)}}. \tag{51}$$

Furthermore, we introduce a power allocation factor defined in [21] to denote the ratio between optical power of adjacent layers in LGABO-OFDM. This factor is given by

$$\alpha_l \triangleq \frac{P_{\mathrm{o},l}}{P_{\mathrm{o},l+1}} = \frac{\beta_l\sqrt{M_{l+1}/\left(m_{l+1}-1\right)}}{\beta_{l+1}\sqrt{M_l/\left(m_l-1\right)}},\ 1 \le l \le L-1. \tag{52}$$

Especially, when $m_l = 2$ for each layer in LGABO-OFDM, $\alpha_l = \sqrt{2}$ for each pair of adjacent layers, which corresponds with the power allocations in LACO-OFDM [27].

V. Principle of Subcarrier Allocation in LGABO-OFDM

In this section, the principle of subcarrier allocation in LGABO-OFDM is discussed to reach the optimal BER performance and improve the power efficiency with a fixed spectral efficiency and a fixed number of layers. As mentioned above, the subcarrier allocation is governed by the parameter $\vec{m}$. Several $\vec{m}$ could be adopted for a fixed L and M_L, which determine the total number of layers and utilized subcarriers, respectively. Normalized optical bit energy to noise power ratio $E_{b(\mathrm{opt})}/N_0$ proposed in [28] is adopted when evaluating the BER performance of LGABO-OFDM, which is defined as

$$\left(E_{b(\mathrm{opt})}/N_0\right)_{\mathrm{norm}} = \frac{E^2\left\{s_n\right\}}{E\left\{s_n^2\right\}}\left(E_{b(\mathrm{elect})}/N_0\right)_{\mathrm{norm}}, \tag{53}$$

where

$$E_{b(\mathrm{opt})} = E\left\{s_n\right\}/R_b, \tag{54}$$
$$E_{b(\mathrm{elect})} = E\left\{s_n^2\right\}/R_b. \tag{55}$$

In (54) and (55), R_b denotes the average transmitted bit rate. Simple proportion is adopted in (53), where signals are normalized for unity optical power.

Nevertheless, the desired transmitted signal is x_n and the key factor determining BER performance is presented as

$$\left(E_{b(\mathrm{elect,x})}/N_0\right)_{\mathrm{norm}} = \frac{E\left\{x_n^2\right\}}{E^2\left\{s_n\right\}}\left(E_{b(\mathrm{opt})}/N_0\right)_{\mathrm{norm}}, \tag{56}$$

where

$$E_{b(\mathrm{elect,x})} = E\left\{x_n^2\right\}/R_b. \tag{57}$$

Utilizing the optical power allocation method proposed in Section IV, each occupied subcarrier has the same SNR and the average electrical power of $\left(1-\frac{1}{M_L}\right)N$ subcarriers is

$$E\left\{|X_k|^2\right\} = \frac{P_{\mathrm{o}}^2}{A^2} = \frac{E^2\left\{s_n\right\}}{A^2},\ k \in \mathbb{K}^{(l)},\ 1 \le l \le L, \tag{58}$$

which is obtained according to (42), (43), and (49b). Therefore, the average electrical power of x_n could be calculated as

$$E\left\{x_n^2\right\} = \left(1-\frac{1}{M_L}\right)E\left\{|X_k|^2\right\} = \frac{M_L-1}{A^2M_L}E^2\left\{s_n\right\}, \tag{59}$$

where Parseval's theorem is utilized.

Substituting (59) into (56), the normalized electrical bit energy to noise power ratio is given by

$$\left(E_{b(\mathrm{elect,x})}/N_0\right)_{\mathrm{norm}} = \frac{M_L-1}{A^2M_L}\left(E_{b(\mathrm{opt})}/N_0\right)_{\mathrm{norm}}. \tag{60}$$

Let $T = \frac{M_L-1}{A^2M_L}$, it could be inferred that T is another significant parameter in LGABO-OFDM and governs the BER performance. Furthermore, a larger value of T leads to lower BER of LGABO-OFDM at the same normalized optical bit energy to noise power ratio $E_{b(\mathrm{opt})}/N_0$, which helps to design $\vec{m}$ for better BER performance.

For instance, several $\vec{m}$ and the corresponding T are listed in Table 2. It could be found that the LGABO-OFDM system with $\vec{m} = (2,4,8)$ has the lowest BER among the listed 7 LGABO-OFDM OWC systems. The BER performance of the O-OFDM schemes in Table 2 is shown in Fig. 10 in Section VI, which validates the conclusion mentioned above.

TABLE 2. Values of Parameter T for Different LGABO-OFDM Systems

$\vec{m}$	(2,4,8)	(4,4,4)	(4,2,8)	(2,8,4)	(4,8,2)	(8,2,4)	(8,4,2)
T	0.3112	0.3092	0.3056	0.3019	0.2982	0.2878	0.2860

TABLE 3. Parameter Values for Simulations

Parameter	Value
N	1024
Modulation scheme	256-QAM, 16-PAM
Clipping ratio of nonlinear distortion	14 dB

VI. Numerical Results

In this section, we mainly evaluate power efficiency and the capability of resisting the nonlinear distortion. We present numerical results of BER and PAPR performance for the proposed LGABO-OFDM and other conventional optical OFDM schemes for comparison with the number of total subcarriers as $N = 1024$. The symbols on subcarriers are modulated by QAM or PAM. The parameter values for simulations are listed in Table 3. In the channel model introduced in [24], the electrical SNR is given by

$$\mathrm{SNR}_e = \frac{R^2P_t^2h^2}{\sigma_w^2}, \tag{61}$$

where P_t denotes the average optical power of s_n. For a fair comparison, the values of R and h are the same for all the O-OFDM schemes by adopting the same OWC channel.

This article has been accepted for publication in IEEE Open Journal of the Communications Society. This is the author's version which has not been fully edited and content may change prior to final publication. Citation information: DOI 10.1109/OJCOMS.2024.3400316

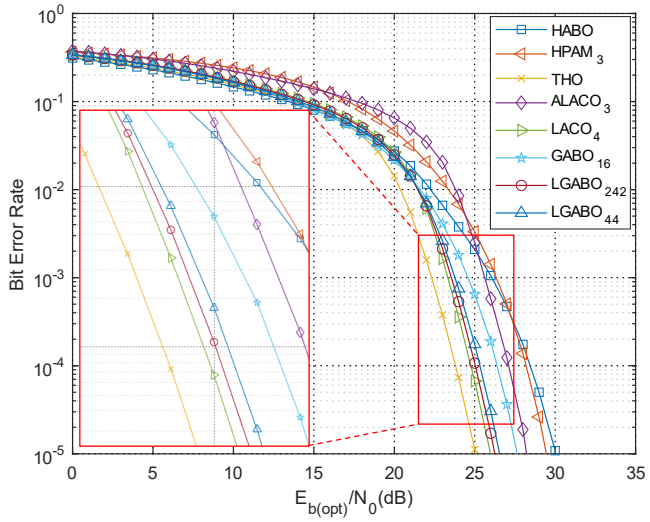

FIGURE 9. BER performance of various optical OFDM schemes versus $E_{b(\mathrm{opt})}/N_0$.

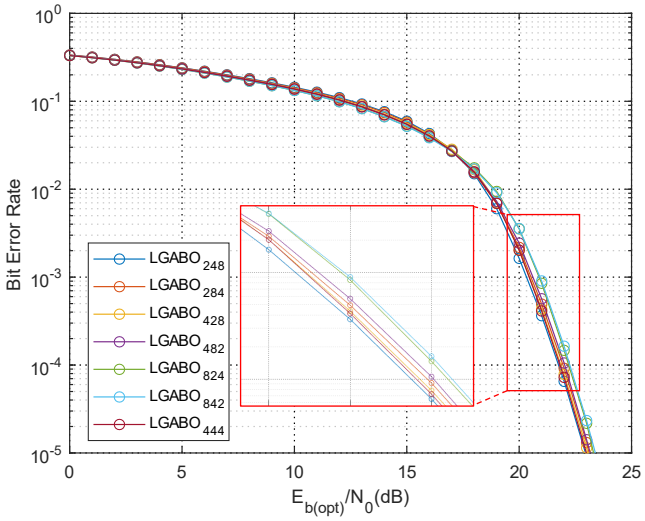

FIGURE 10. BER performance of various LGABO-OFDM schemes versus $E_{b(\mathrm{opt})}/N_0$.

A. BER Performance

The BER performance of various optical OFDM schemes is evaluated by utilizing $E_{b(\mathrm{opt})}/N_0$ similarly to [28] and presented in Fig. 9. 256-QAM and 16-PAM are utilized in these O-OFDM schemes. To obtain the same spectral efficiency, we evaluate the BER performance of HPAM-DMT with $G = 3$, ALACO-OFDM with 3 layers, LACO-OFDM with 4 layers, GABO-OFDM with $m = 16$, and LGABO-OFDM with $\vec{m}_1 = (2, 4, 2)$ and $\vec{m}_2 = (4, 4)$. The parameter G is defined in [20] and it implies that $\left(1 - 2^{G+1}\right)$ of the spectral resources are occupied in HPAM-DMT.

Regarding LACO-OFDM and GABO-OFDM as special cases of LGABO-OFDM with $\vec{m} = (2, 2, 2, 2)$ and $\vec{m} = (16)$, we can observe that the proposed LGABO-OFDM is superior to HABO-OFDM, HPAM-DMT, and ALACO-OFDM in BER performance. Furthermore, LGABO-OFDM with fewer layers leads to a higher BER since a larger value of m corresponds to larger adaptive biases, larger signal power, and larger noise power at the same $E_{b(\mathrm{opt})}/N_0$.

Additionally, Fig. 10 presents the BER performance of several LGABO-OFDM schemes with $L = 3$ and $M_L = 64$, which corresponds to Table 2 in Section V exactly.

It can be seen in Fig. 9 that LGABO-OFDM has higher BER than THO-OFDM. However, the performance gap is small and acceptable due to the higher spectral efficiency of LGABO-OFDM. To take both BER performance and spectral efficiency into account similarly to [29], we plot $< E_{b(\mathrm{opt})}/N_0 >_{\mathrm{BER}}$ versus bit rate/normalized bandwidth in Fig. 11 for various optical OFDM schemes including HABO-OFDM, HPAM-DMT with $G = 3$, THO-OFDM, ALACO-OFDM with $L = 3$, LACO-OFDM with $L = 4$, GABO-OFDM with $m = 16$, and LGABO-OFDM with $\vec{m}_1 = (2, 4, 2)$ and $\vec{m}_2 = (4, 4)$. In each optical OFDM scheme, we adopt 4-QAM, 16-QAM, 64-QAM, 256-QAM, and 1024-QAM while 2-PAM, 4-PAM, 8-PAM, 16-PAM, and 32-PAM are utilized correspondingly. In this figure, $< E_{b(\mathrm{opt})}/N_0 >_{\mathrm{BER}}$ denotes the required $E_{b(\mathrm{opt})}/N_0$ for the target BER of 10^{-3} while bit rate/normalized bandwidth is obtained by the constellations and spectral efficiency. It can be observed that the required $E_{b(\mathrm{opt})}/N_0$ of LGABO-OFDM is lower than most conventional schemes to maintain the BER to 10^{-3} over the transmission. For instance, the required $E_{b(\mathrm{opt})}/N_0$ of LGABO-OFDM with $\vec{m}_2 = (4, 4)$ is approximately 4dB lower than that of HABO-OFDM. Therefore, to reach the same data rate and 10^{-3} BER target for OWC systems, the communication power consumption of LGABO-OFDM is almost 60.19% lower than that of HABO-OFDM. In addition, it could be inferred that the slopes of HABO-OFDM and THO-OFDM curves are larger than other optical OFDM schemes on account of their lower spectral efficiency. The numerical results imply that the proposed LGABO-OFDM requires lower power than its counterparts to achieve the same BER target with the same spectral efficiency, which demonstrates higher power efficiency of LGABO-OFDM.

B. PAPR Performance

In IM/DD-based OWC systems, optical devices such as power amplifiers and LEDs at the transmitter side have limited linear range and will suffer severe nonlinear distortion from time-domain signals with high PAPR. Optical OFDM schemes with lower PAPR possess greater resistance to nonlinear distortion by keeping the transmitted time-domain signal values within the linear range of the optical devices, which is therefore essential for OWC systems.

Fig. 12 presents the PAPR performance of various optical OFDM schemes. It can be observed that the proposed LGABO-OFDM has relatively lower PAPR. For example, the PAPR of LGABO-OFDM with $\vec{m} = (4, 4)$ is approximately 2 dB and 1.7 dB lower than that of THO-OFDM and LACO-

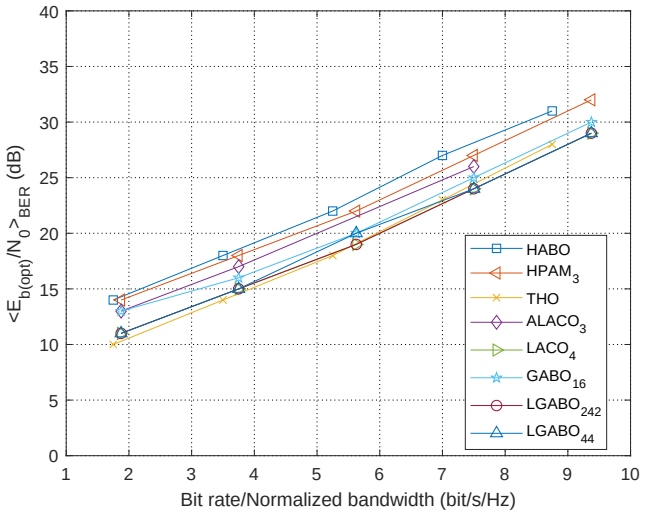

FIGURE 11. The required $E_{b(\mathrm{opt})}/N_0$ for 10^{-3} BER target versus bit rate/normalized bandwidth.

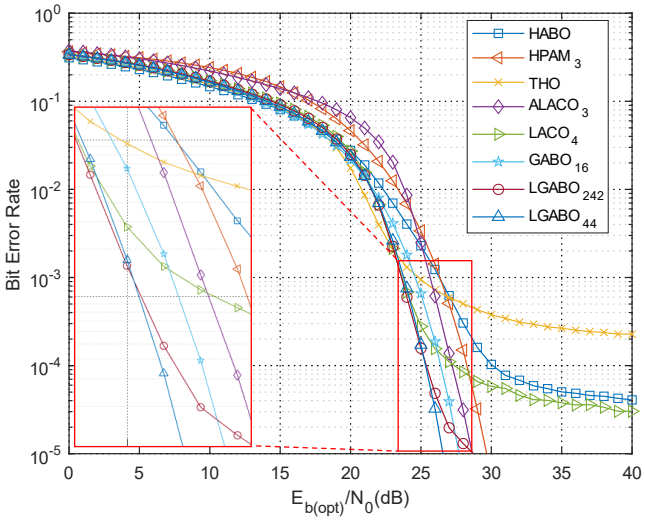

FIGURE 13. BER performance with nonlinear distortion.

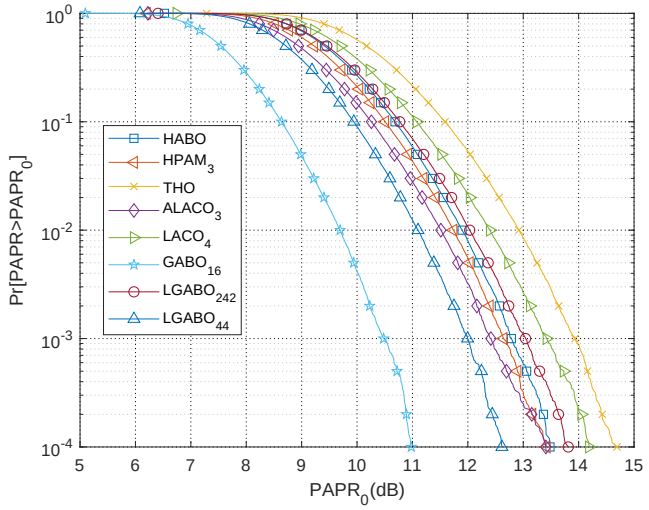

FIGURE 12. PAPR curves of various optical OFDM schemes.

OFDM, respectively. Therefore, LGABO-OFDM performs better when resisting the nonlinear distortion introduced in [30]. It also implies that LGABO-OFDM with few layers, i.e., LGABO-OFDM$_{44}$ corresponds to a lower PAPR since a larger value of parameter m leads to relatively larger adaptive bias and higher average power of LGABO-OFDM.

By incorporating the double-sided clipping model of the nonlinear optical modulation introduced in [31], [32], we evaluate the BER performance with nonlinear distortion for various optical OFDM schemes as shown in Fig. 13 with 14 dB clipping ratio. Compared with the resulting curves without nonlinear distortion as in Fig. 9, significant performance losses appear in HABO-OFDM, THO-OFDM, and LACO-OFDM schemes, whose BER could not decrease to zero when $E_{b(\mathrm{opt})}/N_0$ increases up to 40 dB. The error floors of these optical OFDM schemes are caused by the clipped noise at both sides in nonlinear optical devices. Nevertheless, less performance decline resulting from nonlinear distortion could be distinguished in the proposed LGABO-OFDM with $\vec{m} = (4, 4)$, GABO-OFDM, and ALACO-OFDM, and HPAM-DMT especially in the regime of high $E_{b(\mathrm{opt})}/N_0$. It results from their relatively low PAPR and demonstrates the capability of resisting the nonlinear distortion. We can see that the proposed LGABO-OFDM maintains lower BER and higher power efficiency than its counterparts when nonlinear distortion is introduced. Considering all the facts mentioned above, the proposed LGABO-OFDM is a potentially promising optical OFDM scheme for OWC systems.

VII. Conclusion

In this paper, we proposed a novel LGABO-OFDM scheme for OWC systems in which subcarriers are divided into several layers and transmitted simultaneously and designed an iterative receiver to recover the transmitted information. In order to further improve the power efficiency with fixed spectral efficiency, a novel method of optical power allocation and the principle of subcarrier allocation in LGABO-OFDM are proposed according to the analysis of the statistical properties of the adaptive bias. Additionally, theoretical analysis has proved the lower complexity of LGABO-OFDM compared with LACO-OFDM. Numerical results indicate that LGABO-OFDM has lower BER and higher power efficiency than HABO-OFDM, HPAM-DMT, and ALACO-OFDM schemes. Furthermore, lower PAPR of the proposed LGABO-OFDM demonstrates better performance than its counterparts when resisting the nonlinear distortion. Since the parameter m in each layer of LGABO-OFDM is not a constant, it is plausible to increase the flexibility for OWC system design with optical OFDM schemes.

REFERENCES

[1] A. Al-Kinani, C.-X. Wang, L. Zhou, and W. Zhang, "Optical wireless communication channel measurements and models," *IEEE Commun. Sur. & Tut*, vol. 20, no. 3, pp. 1939–1962, 3rd Quarter 2018.

[2] H. Mei, J. Ding, J. Zheng, X. Chen, and W. Liu, "Overview of vehicle optical wireless communications," *IEEE Access*, vol. 8, pp. 173461-173480, 2020.
[3] H. Elgala, R. Mesleh, H. Haas, and B. Pricope, "OFDM visible light wireless communication based on white LEDs," in *Proc. IEEE 65th Vehicular Technology Conference (VTC2007-Spring)*, 2007, pp. 2185–2189.
[4] J. Gancarz, H. Elgala, and T. D. C. Little, "Impact of lighting requirements on VLC systems," *IEEE Commun. Mag.*, vol. 51, no. 12, pp. 34–41, Dec. 2013.
[5] X. -Y. Xu and D. -W. Yue, "A novel non-Hermitian symmetry orthogonal frequency division multiplexing system for visible light communications," *IEEE Photon. J.*, vol. 13, no. 6, pp. 1–9, Dec. 2021.
[6] C. Chen, W. Zhong, and D. Wu, "Non-Hermitian symmetry orthogonal frequency division multiplexing for multiple-input multiple-output visible light communications," *J. Opt. Commun. Netw.*, vol. 9, pp. 36–44, Dec. 2017.
[7] X. Zhang, T. Van Luong, P. Petropoulos, and L. Hanzo, "Machine-learning-aided optical OFDM for intensity modulated direct detection," *J. Lightwave Technol.*, vol. 40, no. 8, pp. 2357–2369, Apr. 2022.
[8] J. B. Carruthers and J. M. Kahn, "Multiple-subcarrier modulation for nondirected wireless infrared communication," *IEEE J. Sel. Areas Commun.*, vol. 14, no. 3, pp. 538–546, Apr. 1996.
[9] J. Armstrong, "OFDM for optical communications," *J. Lightwave Technol.*, vol. 27, no. 3, pp. 189–204, Feb. 2009.
[10] S. C. J. Lee, S. Randel, F. Breyer, and A. M. J. Koonen, "PAM-DMT for intensity-modulated and direct-detection optical communication systems," *IEEE Photon. Technol. Lett.*, vol. 21, no. 23, pp. 1749–1751, Dec. 2009.
[11] B. Ranjha and M. Kavehrad, "Hybrid asymmetrically clipped OFDM-based IM/DD optical wireless system," *J. Opt. Commun. Netw.*, vol. 6, no. 4, pp. 387–396, Apr. 2014.
[12] T. Zhang, L. Sun, C. Zhao, S. Qiao, and Z. Ghassemlooy, "Low-complexity receiver for HACO-OFDM in optical wireless communications," *IEEE Wireless Commun. Lett.*, vol. 10, no. 3, pp. 572–575, Mar. 2021.
[13] Q. Wang, C. Qian, X. Guo, Z. Wang, D. G. Cunningham, and I. H. White, "Layered ACO-OFDM for intensity-modulated direct-detection optical wireless transmission," *Opt. Express*, vol. 23, no. 9, pp. 12382–12393, May 2015.
[14] Q. Wang, Z. Wang, X. Guo, and L. Dai, "Improved receiver design for layered ACO-OFDM in optical wireless communications," *IEEE Photon. Technol. Lett.*, vol. 28, no. 3, pp. 319–322, Feb. 2016.
[15] R. Bai, Q. Wang and Z. Wang, "Asymmetrically clipped absolute value optical OFDM for intensity-modulated direct-detection systems," *J. Lightwave Technol.*, vol. 35, no. 17, pp. 3680–3691, Sept. 2017.
[16] R. Bai and S. Hranilovic, "Layered antisymmetry-constructed clipped optical OFDM for low-complexity VLC systems," *Opt. Express*, vol. 29, pp. 10613–10630, Mar. 2021.
[17] B. Li, W. Xu, Z. Li, and Y. Zhou, "Adaptively biased OFDM for IM/DD-aided optical wireless communication systems," *IEEE Wireless Commun. Lett.*, vol. 9, no. 5, pp. 698–701, May 2020.
[18] Z. Geng, F. Yang, Z. Li, and Y. Dong, "Generalized adaptively biased optical OFDM for optical wireless communications," in *Proc. SPIE 12066, Applied Optics and Photonics China (AOPC) 2021: Micro-optics and MOEMS*, 120661H, 2021.
[19] B. Li, X. Xue, S. Feng, and W. Xu, "Layered optical OFDM with adaptive bias for dimming compatible visible light communications," *J. Lightwave Technol.*, vol. 39, no. 11, pp. 3434–3444, Jun. 2021.
[20] B. Li, S. Feng, and W. Xu, "Spectrum-efficient hybrid PAM-DMT for intensity-modulated optical wireless communication," *Opt. Express*, vol. 28, pp. 12621–12637, 2020.
[21] R. Bai and S. Hranilovic, "Absolute value layered ACO-OFDM for intensity-modulated optical wireless channels," *IEEE Trans. Commun.*, vol. 68, no. 11, pp. 7098–7110, Nov. 2020.
[22] H. Hong and Z. Li, "Hybrid adaptive bias OFDM-based IM/DD visible light communication system," *Photonics*, vol. 8, no. 7, 2021.
[23] T. Zhang, H. Ji, Z. Ghassemlooy, X. Tang, B. Lin, and S. Qiao, "Spectrum-Efficient Triple-Layer Hybrid Optical OFDM for IM/DD-Based Optical Wireless Communications," *IEEE Access*, vol. 8, pp. 10352-10362, 2020.
[24] M. T. Dabiri, S. M. S. Sadough, and M. A. Khalighi, "Channel modeling and parameter optimization for hovering UAV-based free-space optical links," *IEEE J. Sel. Areas Commun.*, vol. 36, no. 9, pp. 2104-2113, Sept. 2018.
[25] J. Kahn and J. Barry, "Wireless infrared communications," *Proc. IEEE*, vol. 85, no. 2, pp. 265–298, 1997.
[26] X. Liu, J. Zhou, N. Huang, and W. Zhang, "Improved receivers for optical wireless OFDM: an information theoretic perspective," *IEEE Trans. Commun.*, vol. 70, no. 7, pp. 4439–4453, Jul. 2022.
[27] X. Zhang, Q. Wang, R. Zhang, S. Chen, and L. Hanzo, "Performance analysis of layered ACO-OFDM," *IEEE Access*, vol. 5, pp. 18366–18381, Aug. 2017.
[28] J. Armstrong, B. J. C. Schmidt, D. Kalra, H. A. Suraweera, and A. J. Lowery, "SPC07-4: Performance of asymmetrically clipped optical OFDM in AWGN for an intensity modulated direct detection system," in *Proc. IEEE Globecom*, 2006, pp. 1–5.
[29] S. D. Dissanayake and J. Armstrong, "Comparison of ACO-OFDM, DCO-OFDM and ADO-OFDM in IM/DD systems," *J. Lightwave Technol.*, vol. 31, no. 7, pp. 1063–1072, Apr. 2013.
[30] H. Elgala, R. Mesleh, and H. Haas, "A study of LED nonlinearity effects on optical wireless transmission using OFDM," in *Proc. IFIP International Conference on Wireless and Optical Communications Networks (WOCN)*, 2009, pp. 1–5.
[31] H. Zhang, Y. Yuan, and W. Xu, "PAPR reduction for DCO-OFDM visible light communications via semidefinite relaxation," *IEEE Photon. Technol. Lett.*, vol. 26, no. 17, pp. 1718–1721, Sept. 2014.
[32] B. Li, W. Xu, H. Zhang, C. Zhao, and L. Hanzo, "PAPR reduction for hybrid ACO-OFDM aided IM/DD optical wireless vehicular communications," *IEEE Trans. Veh. Technol.*, vol. 66, no. 10, pp. 9561–9566, Oct. 2017.

Zuhang Geng (Student Member, IEEE) received the B.S. degree in electronic engineering from Tsinghua University, Beijing, China in July 2019. Currently, he is with the Ph.D program of information and communication engineering of Shenzhen International Graduate School, Tsinghua University, Shenzhen, China. His research interests include optical wireless communication, optical OFDM and OTFS schemes, and unmanned aerial vehicle-based communication.

Xinke Tang received the M.Res. and Ph.D. degrees from the University of Cambridge, Cambridge, U.K., in 2014 and 2019, respectively. He is currently an Associate Professor with Peng Cheng Laboratory. His research interests include optical wireless communication, optical networks, optical switching, and quantum key distribution.

Yuhan Dong (Senior Member, IEEE) received the B.S. and M.S. degrees in electronic engineering from Tsinghua University, Beijing, China, in 2002 and 2005, respectively, and the Ph.D. degree in electrical engineering from North Carolina State University, Raleigh, NC, USA, in 2009.

Since January 2010, he has been with the Shenzhen International Graduate School, Tsinghua University, where he is currently an Associate Professor and a member of the Modern Communication Laboratory. His research interests include wireless communications and networking, machine learning and optimization, and optical wireless communications. He was a recipient of the 2008 IEEE GLOBECOM Best Paper Award.